



Contents lists available at ScienceDirect

## Arabian Journal of Chemistry

journal homepage: [www.ksu.edu.sa](http://www.ksu.edu.sa)

# Nattokinase enhances the sensitivity of cancer cells to oxaliplatin through mitochondrial pathway and induction of apoptosis

Yong-Po Zhang<sup>a</sup>, Yue-Wei Tian<sup>a</sup>, Jiang Geng<sup>b</sup>, Xin-Hui Zhou<sup>a</sup>, Meng-Ze Li<sup>a</sup>, Guang-Huan Liu<sup>a</sup>, Chun-Yan Gao<sup>a,\*</sup>, Ai-Qin Yue<sup>c</sup>, Jin-Zhong Zhao<sup>a,\*</sup>, Wei-Jun Du<sup>c,\*</sup>

<sup>a</sup> Department of Basic Sciences, Shanxi Agricultural University, Taiyuan, Shanxi 030801, PR China

<sup>b</sup> Shanxi Provincial Cancer Hospital, Taiyuan, Shanxi 030012, PR China

<sup>c</sup> College of Agronomy, Shanxi Agricultural University, Taiyuan, Shanxi 030801, PR China

## ARTICLE INFO

## Keywords:

Oxaliplatin  
Nattokinase  
Combination  
Anticancer  
Mitochondrial pathway

## ABSTRACT

Combination therapy consisting of anticancer drugs has been used to decrease the adverse effects and increase the effectiveness of the drugs. The present study aimed to examine the synergistic effect and potential mechanisms of oxaliplatin and nattokinase (NK) combined treatment for BGC-823, HepG-2, HeLa, and NCI-H460 cells. NK was isolated and purified from black soybean natto by dialysis and gel filtration chromatography, which had a nattokinase activity of 600,391 U/g. MTT experiment, clone formation assay, Hoechst 33,342 staining, DCFH-DA staining, and JC-1 staining showed that NK had no cytotoxicity and oxaliplatin could inhibit cell proliferation. Oxaliplatin combined with NK could enhance its anticancer effect and lead to mitochondrial dysfunction by causing the increase of intracellular ROS, which eventually induced apoptosis. Compared to oxaliplatin alone, nattokinase in combination with oxaliplatin can effectively inhibit DNA synthesis and increase cell uptake, ultimately inhibiting cell proliferation. Transwell and angiogenesis experiments proved that the combination of NK and oxaliplatin could more effectively inhibit cell migration, invasion, and in vitro angiogenesis, thereby preventing the spread and metastasis of tumors. RT-qPCR showed that the mechanism of inhibition of cell proliferation and thus induction of apoptosis by the combination of NK and oxaliplatin may be achieved through the upregulation of BAD, BAX, and Caspase-3 genes. Molecular docking results show that NK could act as the carrier of oxaliplatin. In conclusion, the above results suggested that NK could play a synergistic anticancer role with oxaliplatin by inducing apoptosis through the mitochondrial pathway, enhance the sensitivity of cancer cells to oxaliplatin, and provide a new strategy for cancer treatment.

## 1. Introduction

Cancer, the leading cause of death worldwide, has become a serious threat to human life and health. The incidence of cancer is on the rise in countries around the world due to the effects of smoking, unhealthy diet, physical inactivity, growth and aging of the population (Thun et al., 2010). According to statistics, 19.3 million new cases and 10 million cancer deaths have occurred in 2020. Among them, lung, liver, stomach, and breast cancers are the main cancers that cause death (Sung et al.,

2021). Surgery, radiotherapy, and chemotherapy are the main options for cancer treatment at present. In addition, there are more new developments in the research of cancer treatment through targeted therapy and immunotherapy (Zhang et al., 2022). Surgery plays a pivotal role in early stages of cancer, but it is less effective for advanced stages and carries associated risks (Petrella et al., 2022). Chemotherapy and radiotherapy, however, can have certain side effects, such as permanent alopecia (Freites-Martinez et al., 2019), impairment of taste (Kiss et al., 2021), nausea and vomiting (Ruhlmann and Herrstedt, 2016), etc.

**Abbreviations:** DCFH-DA, 2',7'-dichlorofluorescein diacetate; DCFH, 2',7'-dichlorodihydrofluorescein; DCF, 2',7'-dichlorofluorescein; DMSO, dimethyl sulfoxide; FBS, fetal bovine serum; FCM, flow cytometry; FI, fold increase; IC<sub>50</sub>, 50% inhibiting concentration; ICP-OES, inductively coupled plasma optical emission spectrometer; MMP, mitochondrial membrane potential; MTT, thiazolyl blue tetrazolium bromide; NK, nattokinase; OD, optical density; OXA, Oxaliplatin; ROS, reactive oxygen species; RT-qPCR, real-time quantitative polymerase chain reaction. SEM, scanning electron microscopy.

Peer review under responsibility of King Saud University.

\* Corresponding authors.

E-mail addresses: [gaocy@sxau.edu.cn](mailto:gaocy@sxau.edu.cn) (C.-Y. Gao), [zhaojz@sxau.edu.cn](mailto:zhaojz@sxau.edu.cn) (J.-Z. Zhao), [duweijun@sxau.edu.cn](mailto:duweijun@sxau.edu.cn) (W.-J. Du).

<https://doi.org/10.1016/j.arabjc.2023.105478>

Received 22 July 2023; Accepted 22 November 2023

Available online 23 November 2023

1878-5352/© 2023 The Authors. Published by Elsevier B.V. on behalf of King Saud University. This is an open access article under the CC BY-NC-ND license (<http://creativecommons.org/licenses/by-nc-nd/4.0/>).

Although targeted therapy and immunotherapy also offer more options for patients with advanced cancer, they still cannot stop the trend of rapid cancer progression (Guo et al., 2021a, 2021b). Without the development of new ways to prevent, delay or treat cancer, the number of cancer-related deaths will continue to increase.

However, it is worth mentioning that in clinical medicine, cancer and thrombus often do not occur separately, but interact and reinforce each other (Leal et al., 2017). When the coagulation and anticoagulation systems in the body lose balance, blood components will be converted into blood clots, which are called thrombus. Complications from thrombus turn into the second leading cause of death in patients with cancer. On the one hand, the tissue factor (TF) and cancer procoagulant (CP) produced by cancer cells promote thrombosis (Liu et al., 2022), and the application of chemotherapeutic drugs increases the risk of thrombosis (Grover et al., 2021). On the other hand, the formation of thrombus can also cause the occurrence of lesions such as hypoxia and necrosis in the tissues at the site of thrombus, which increases the chance of cancer (Prodger et al., 2016). Therefore, the relevance of cancer to thrombotic disease has attracted widespread clinical attention. Treating cancer alongside and preventing and inhibiting thrombosis not only reduces the incidence of thrombotic complications but also improves the tumor environment, offering a new strategy for the treatment of cancer and thrombosis (Rickles, 2006). In recent years, combination therapies have been attracting a lot of interest in the field of anticancer research. By playing the synergistic and complementary roles of drugs, the combination of drugs can achieve the purpose of increasing the anticancer effect of drugs while reducing the complications and toxic side effects caused by cancer (Pearson et al., 2023). Studies related to the combination therapies for cancer treatment have also been reported in previous researches. It has been discovered that glutathione (GSH) combined with cisplatin (CDDP) and oxaliplatin (OXA) could inhibit growth in A549 cells and induce apoptosis (Xu et al., 2010). Other studies have shown that combinations such as bithionol and cisplatin could enhance ovarian cancer chemosensitivity (Ayyagari et al., 2017). A recent study also revealed the potential anticancer activities of the combination of sulfamethoxazole and quercetin on MCF-7, HepG2, HCT-116, and PC3 cell lines via the induction of the apoptotic pathway (Sahyon et al., 2022). In addition, Shrey Modi's results suggested that triptolide sensitize pancreatic cancer cells to oxaliplatin (Modi et al., 2015). All of the above studies prove that combination therapy is feasible in anticancer treatment.

Oxaliplatin is a third-generation platinum complex with broad in vitro anticancer activity and in vivo antitumor effects (Mowaka and Linscheid, 2008). Previous studies by investigators have determined that oxaliplatin is an important broad spectrum anticancer drug used in a variety of tumor model systems for the treatment of stomach (Sato, 2015), liver (Wang et al., 2009), lung (Jin et al., 2020), as well as cervical cancer (He et al., 2022). However, resistance to oxaliplatin is also becoming known, which limits its clinical application. Based on the above, it is imperative to find a way to ensure the efficacy and enhance the sensitivity of cancer cells to oxaliplatin.

Nattokinase (NK) is an alkaline protease consisting of 275 amino acid residues isolated from the traditional fermented food natto (Chen et al., 2018). Some trials have demonstrated that NK has potent fibrinolytic and antithrombotic activity, both in animal and human studies (Yan et al., 2021; Hodis et al., 2021; Sheng et al., 2023). A recent study revealed intratumoral injection of NK could modulate solid tumor microenvironment via direct degradation of fibronectin and indirect inhibition of cancer-associated fibroblast activity (Zhang et al., 2023a, 2023b). To the best of our knowledge, the combined treatment of oxaliplatin with NK has not been reported in literature. Consequently, the purpose of our study is to determine whether NK can improve the sensitivity of cancer cells to oxaliplatin and the possible mechanisms. In our experiments, we confirmed that nattokinase itself has no significant cytotoxicity, and when combined with oxaliplatin, the cytotoxicity is significantly superior to that of oxaliplatin alone, resulting in a "0 + 1 >

1" efficacy. The development of a new strategy for the treatment of cancer with oxaliplatin and NK is of great significance and may provide new ideas for cancer treatment, especially for the combined treatment of cancer and its thrombotic complications.

## 2. Materials and methods

### 2.1. Materials

Huguan black soybeans were obtained from the genetics and germplasm innovation lab of Shanxi Agricultural University. Natto bacteria powder was from Guangdong Shunde Shangchuan biotechnology company. Dimethyl sulfoxide (DMSO), HNO<sub>3</sub>, H<sub>2</sub>O<sub>2</sub>, HCl, CHCl<sub>3</sub>, C<sub>3</sub>H<sub>7</sub>OH, and C<sub>2</sub>H<sub>5</sub>OH were purchased from Aladdin. Urokinase, thrombin from bovine plasma, fibrinogen, agarose, RPMI-1640 medium, DMEM medium, fetal bovine serum (FBS), trypsin-EDTA solution, 3-(4, 5-dimethylthiazol-2-yl)-2, 5-diphenyl tetrazolium bromide (MTT), crystal violet, paraformaldehyde (4 %), Hoechst 33342 (Cat. No. B8040; ex/em = 350/461 nm), 2',7'-dichlorofluorescein diacetate (DCFH-DA, Cat. No. D6470; ex/em = 504/529 nm), mitochondrial membrane potential assay kit with JC-1 (Cat. No. M8650; monomer, ex/em = 490/530 nm; aggregates, ex/em = 525/590 nm), transwell chambers, and oxaliplatin were all provided from Solarbio. The cell cycle kit (Cat. No. CA1510) and Caspase Inhibitor Z-VAD-FMK (Cat No. C1202) were from Beyotime. The matrigel matrix was obtained from Corning. The transzol up (Lot#P40814), transscript®one-step gDNA removal and cDNA synthesis supermix (Lot#P20414) and transstart®tip green qPCR supermix (Lot#Q20922) were from TransGen Biotech.

Constant temperature and humidity incubator (LRHS-150-III) was from Shanghai Yuejin Medical Equipment Company, vacuum freeze dryer (ATS.D5-2 M) was from Keyi Chuangzhi (Beijing) Technology Development Company, the inverted fluorescence optical microscope (DMIL LED) was from Leica Microsystems Trading (Shanghai) Company, enzyme analyzer (DNM-9602) was from Beijing Planck New Technology Company, ultra clean bench (SW-CJ-1D) was from Suzhou Purifying Equipment Company, the CO<sub>2</sub> cell incubator (Galaxy 170S) was from England NEW BRUNSWIC, the ICP-OES (ICPE-9820) was from Japan SHIMADZU, the FCM (BD Accuri C6 Plus) was from America Becton Dickinson, and the real-time fluorescence quantitative PCR instrument (CFX96) was from America Bio-Rad.

### 2.2. Cell culture

Human gastric carcinoma (BGC-823), hepatocellular carcinoma (HepG-2), cervical carcinoma (HeLa), non-small cell lung carcinoma (NCI-H460), and umbilical vein endothelial cells (HUVEC) were obtained from the American Type Culture Collection (ATCC, USA). BGC-823 cells, HepG-2 cells, and NCI-H460 cells were cultured in RPMI-1640 medium containing 10 % FBS, while HeLa cells and HUVEC cells were cultured in DMEM medium containing 10 % FBS.

### 2.3. Preparation of NK

Huguan black soybeans were washed 2–3 times with distilled water and soaked overnight before steaming. Then they were inoculated with *Bacillus natto* and fermented in a constant temperature and humidity incubator. The finished black soybean natto was obtained by post-ripening in 4 °C, Black soybean natto was freeze-dried to obtain a lyophilised powder, mixed with saline at a ratio of 1:10 (g: mL), and then centrifuged to obtain the supernatant, which was the crude extract of black soybean nattokinase. A dialysis bag with a MW of 10,000 D was selected for the purification of crude extract based on the molecular weight of NK. After filling the sample, the bags were dialyzed in distilled water for 48 h, with water changes every 2 h. The dialyzed samples were freeze-dried and further purified using dextran gel chromatography according to the method of Devi C S (Devi et al., 2016) to obtain NK.

After adding the Sephadex G-100 to the column, the sample was dissolved and centrifuged to collect the supernatant, which was also added to the column. When all the samples were in the gel, the flow rate was adjusted to the appropriate rate and the eluate was collected. The eluates with NK activity were combined and freeze-dried to get the final target sample, which was NK.

#### 2.4. Enzyme activity and preliminary structural investigation of NK (FTIR)

The NK obtained was assayed for enzymatic activity according to Astrup's (Astrup and Müllertz, 1952) method with some refinements. Fibrinogen solution (2.5 mg/mL) and agar solution (1.5 %) were mixed and poured into culture dish, then 1 mL of thrombin solution (25 U/mL) was added and mixed well. After cooling, a creamy white opaque fibrin plate can be made. For spotting, small well was punched out of the plate and 20  $\mu$ L of NK sample solution (5 mg/mL) was added. When the spotting was completed, the fibrin plate was placed in a constant temperature and humidity incubator for 18 h to react. The diameter of the dissolved circles formed around the small wells on the plate was measured at the end of the reaction and the activity of black bean natokinase was calculated from the standard curve. Urokinase standards were prepared to concentrations of 1000 U/mL, 800 U/mL, 600 U/mL, 400 U/mL, 200 U/mL, 100 U/mL and 50 U/mL. Following the above method, 20  $\mu$ L of urokinase solution was added to each well and the diameter of the dissolved circles was measured and the area calculated after 18 h of reaction. The standard curve was plotted using the urokinase activity as the horizontal coordinate and the area of the dissolved circles as the vertical coordinate.

The preliminary structure of NK was investigated by infrared spectroscopy and scanning electron microscopy. An appropriate amount of NK sample was weighed and mixed with KBr powder at a mass ratio of 1:100, thoroughly ground and pressed. The data were collected by scanning with an infrared spectrometer in the wavelength range of 400 ~ 4000  $\text{cm}^{-1}$  and the characteristic absorption peaks of NK were determined by Fourier Transform infrared spectroscopy (FTIR). The freeze-dried NK powder was glued onto a copper sample stage, the unglued sample powder was blown off. The surface of the sample was sprayed with gold to observe the surface shape of NK by scanning electron microscopy.

To obtain the molecular weight, NK was analyzed by 5 % (stacking gel) and 10 % (separating gel) SDS-PAGE (sodium dodecyl sulfate polyacrylamide gel electrophoresis). The initial voltage is 80 V, and the adjusted voltage is 120 V when the strip is completely into the separator. Stop electrophoresis when the apex strip is 1 cm away from the bottom of the glass plate. The gel was transferred into Coomassie Brilliant Blue R-250 staining solution and washed with water after staining. Then add the destaining solution and shake slowly until the protein bands are clearly visible.

#### 2.5. MTT colorimetric method

Cytotoxicity of NK or/and oxaliplatin was evaluated using the MTT colorimetric method on BGC-823, HepG-2, HeLa, NCI-H460 and HUVEC cells. Cells in the logarithmic phase were seeded into 96-well plates at  $3 \sim 5 \times 10^3$  cells/well, incubated at 37 °C, 5 % CO<sub>2</sub> for a while, and treated with different concentrations of NK or/and oxaliplatin. After incubating for 48 h, MTT (5 mg/mL) was added to the cells and incubated for 4 h. Then the supernatant was sucked off, and 100  $\mu$ L of DMSO was added. After the crystal was dissolved, we could obtain the OD values and IC<sub>50</sub> values.

#### 2.6. Clone formation assay

We used the clone formation assay to test the viability of BGC-823, HepG-2, HeLa, and NCI-H460 cells. Cells in the logarithmic phase

were seeded into 6-well plates at  $1 \times 10^3$  cells/well and incubated at 37 °C, 5 % CO<sub>2</sub> for 10 days. The cells were treated with oxaliplatin alone or in combination with NK and cultured for a period until the clones were visible. After removing the medium, the cells were washed twice with PBS, fixed with 4 % paraformaldehyde for 30 min, and then stained with 0.1 % crystal violet dye for 20 min. The cells were carefully washed with flowing water and then dried under natural air. The cells were photographed and the number of clones was counted by Image J.

#### 2.7. Hoechst 33342 staining

The Hoechst 33,342 staining was employed to study the effect of oxaliplatin alone or in combination with NK on apoptosis in BGC-823, HepG-2, HeLa, and NCI-H460 cells. Cells in the logarithmic phase were seeded into 12-well plates at  $3 \sim 5 \times 10^4$  cells/well and incubated at 37 °C, 5 % CO<sub>2</sub> for 24 h. The cells were treated with oxaliplatin alone or in combination with NK and incubated for 24 h. After that, Hoechst 33342 dye (10  $\mu$ g/mL) was added to the cells and incubated in the dark for 20 min. Then the apoptotic cells with blue fluorescence were observed by fluorescence microscopy.

#### 2.8. DCFH-DA staining

We used the DCFH-DA staining to investigate the effect of oxaliplatin alone or in combination with NK on reactive oxygen species (ROS) levels in BGC-823, HepG-2, HeLa, and NCI-H460 cells. Cells in the logarithmic phase were seeded into 12-well plates at  $3 \sim 5 \times 10^4$  cells/well and incubated at 37 °C, 5 % CO<sub>2</sub> for 24 h. Afterwards the cells were treated with oxaliplatin alone or in combination with NK and incubated for 24 h. Then the fluorescent probe DCFH-DA (10  $\mu$ M) was added to the cells and incubated in the dark for 30 min. In the same way, the cells with green fluorescence were observed by fluorescence microscopy.

#### 2.9. JC-1 assay

We took advantage of the JC-1 assay to measure the change in mitochondria. Cells in the logarithmic phase were seeded into 12-well plates at  $3 \sim 5 \times 10^4$  cells/well and incubated at 37 °C, 5 % CO<sub>2</sub> for 24 h. After that, the cells were treated with oxaliplatin alone or in combination with NK. Then incubating for 24 h, the fluorescent probe JC-1 was added to the cells and incubated in the dark for 20 min. Finally, the cells with red or green fluorescence were observed by fluorescence microscopy.

#### 2.10. Cell cycle

Flow cytometry (FCM) was required to explore the cell cycle of BGC-823, HepG-2, HeLa, and NCI-H460 cells. Cells in the logarithmic phase were seeded into 6-well plates at  $2 \times 10^5$  cells/well and incubated at 37 °C, 5 % CO<sub>2</sub> for 24 h. The cells were treated with oxaliplatin alone or in combination with NK and incubated for 24 h. After that, the cells were washed with PBS, trypsinized, and collected. Subsequently, the cells were fixed overnight in 70 % ethanol at 4 °C. Finally, they were carried out according to the kit (Cat. No. CA1510) instructions and detected by Flow Cytometry (FCM).

#### 2.11. Cellular uptake

Cellular uptake was used to explore the accumulation of platinum (Pt) in BGC-823, HepG-2, HeLa, and NCI-H460 cells. Cells in the logarithmic phase were seeded into 6-well plates at  $2 \times 10^5$  cells/well and incubated at 37 °C, 5 % CO<sub>2</sub> for 24 h. The cells were treated with oxaliplatin alone or in combination with NK and incubated for 24 h. After that, the cells were washed with PBS, trypsinized, and collected. Then the cells were digested with HNO<sub>3</sub> (100  $\mu$ L, 95 °C, and 2 h), H<sub>2</sub>O<sub>2</sub> (50  $\mu$ L, 95 °C, and 1.5 h), and HCl (100  $\mu$ L, 95 °C, and 2 h), respectively. Finally,

**Table 1**  
Primers used for RT-qPCR.

| Gene                           | Primer  | Sequences (5'-3')       |
|--------------------------------|---------|-------------------------|
| GAPDH(Liu et al., 2021)        | Forward | GACCTGACCTGCGGTCTAG     |
|                                | Reverse | AGGAGTGGGTGTCGCTGT      |
| BAD(Yang et al., 2018)         | Forward | CGGAGGATGAGTGACGAGTTTGT |
|                                | Reverse | ATCCCACCAGGACTGGAAGACTC |
| Bax(Luo et al., 2019)          | Forward | AAACTGGTGCTCAAGGCC      |
|                                | Reverse | AAAGTAGGAGAGGAGGCCGT    |
| Caspase-3(Safwat et al., 2021) | Forward | CTCGGTCTGGTACAGATGTGCA  |
|                                | Reverse | CATGGCTCAGAAGCACACAAC   |

the digested cells were diluted with water to 10 mL, and the Pt content was determined by inductively coupled plasma optical emission spectrometer (ICP-OES).

### 2.12. Transwell migration and invasion assay

Transwell assay was used to evaluate the detection of the migration and invasive ability of BGC-823, HepG-2, HeLa, and NCI-H460 cells. Transwell chambers and 24-well plates were used to form a system. Cells in the logarithmic phase were seeded into the upper chamber of a transwell without (transwell migration assay) or with (transwell invasion assay) matrigel matrix at  $2 \sim 3 \times 10^4$  cells/chamber. It is worth mentioning that the matrigel matrix needed to keep at 37°C in advance for 30 min to solidify. Then the cells were treated with oxaliplatin alone or in combination with NK. Medium containing 20 % FBS was added into the lower chamber and incubated at 37 °C, 5 %CO<sub>2</sub> for 24 h. After that, the chambers were fixed with 4 % paraformaldehyde for 30 min and stained with 0.1 % crystal violet dye for 20 min. Finally, the staining cells were observed by inverted microscope.

### 2.13. In vitro angiogenesis assay

We used the HUVEC cells model to evaluate the effects of oxaliplatin alone or in combination with NK on angiogenesis in vitro. Cells in the logarithmic phase were seeded into 96-well plates with matrigel matrix at  $2 \sim 3 \times 10^4$  cells/well, treated with oxaliplatin alone or in combination with NK, and incubated at 37 °C, 5 %CO<sub>2</sub>. It is worth mentioning that the matrigel matrix needed to keep at 37°C in advance for 30 min to

solidify. At 3 h, 6 h, and 9 h, we observed the structure of angiogenesis using the inverted microscope.

### 2.14. Real-time quantitative polymerase chain reaction (RT-qPCR)

RT-qPCR was used to detected related gene expression in BGC-823 cells. Cells in the logarithmic phase were seeded into 24-well plates at  $2 \sim 3 \times 10^4$  cells/well and incubated at 37 °C, 5 %CO<sub>2</sub> for 24 h. The cells were treated with oxaliplatin alone or in combination with NK and incubated for 24 h. After incubation, the medium is discarded and the total RNA is extracted according to the TransZol up (Lot#P40814) instructions, which should be done on ice and using enzyme-free tips, enzyme-free centrifuge tubes and enzyme-free water to prevent contamination or degradation of the RNA. Total RNA was then reverse transcribed using the TransScript® One-Step gDNA Removal and cDNA Synthesis SuperMix to obtain cDNA. cDNA was used as a template for fluorescent quantitative PCR using the TransStart®Tip Green qPCR SuperMix. RT-qPCR was performed using TransStart®Tip Green qPCR SuperMix. Glyceraldehyde-3-phosphate dehydrogenase (GAPDH) was used as the internal reference gene and the primer sequences used are shown in Table 1, which were determined through references. The total volume of the RT-qPCR reaction system was 20 μL. The procedure was pre-denaturation at 94 °C for 30 s and 45 cycles of denaturation at 94 °C for 5 s and annealing at 60 °C for 30 s. The relative expression of the genes was calculated using the  $2^{-\Delta\Delta CT}$  method.

### 2.15. Study on the apoptosis with Z-VAD-FMK

The method of action of the inhibitor was similar to MTT assay, except that after the cells were cultured in 96-well plates for a period of time, NK and OXA was added to the cells for 48 h with and without the inhibitor after pre-treatment with the Caspase inhibitor Z-VAD-FMK for 10 h. The experimental group was divided into OXA group, OXA + NK group, OXA + Z-VAD-FMK group, OXA + NK + Z-VAD-FMK group.

### 2.16. Statistical analysis

Datas were expressed as mean value  $\pm$  standard deviation. IC<sub>50</sub> values were calculated by using SPSS Statistics 17.0 software. Clone

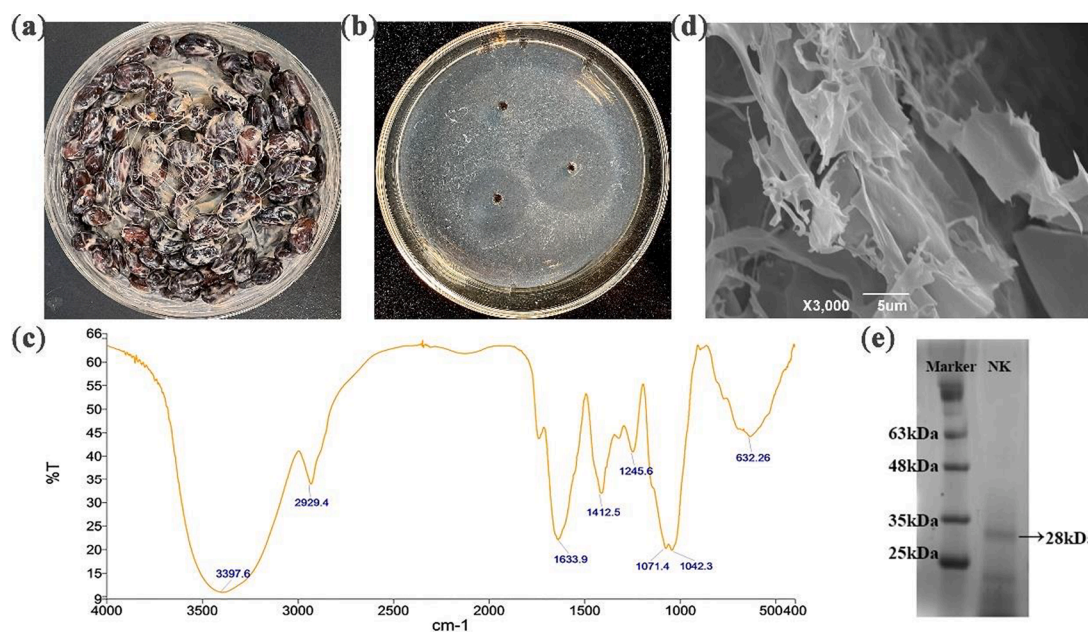


**Fig. 1.** (a) Black soybean natto. (b) The dissolving circle of NK on a fibrin plate. (c) Infrared spectra of NK. (d) SEM images of NK. (e) SDS-PAGE analysis of NK. Lane 1 is the marker protein and lane 2 is NK.

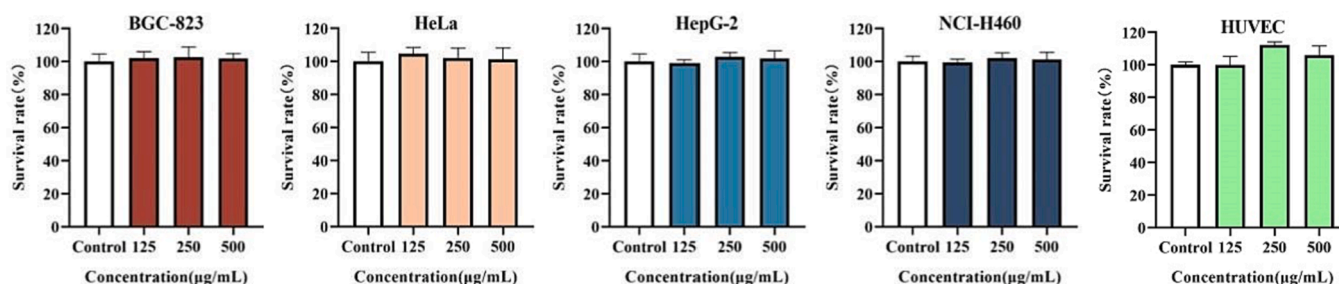


Fig. 2. Survival rate of NK against cells for 48 h. Survival rate (%):  $(OD_{\text{Experiment}} - OD_{\text{Blank}} / OD_{\text{Control}} - OD_{\text{Blank}}) \times 100$  %.

numbers, relative fluorescence intensity, cells numbers, and angiogenesis-related parameters (branch points and capillary length) were analyzed by using Image J software. ANOVA was used for statistical significance analysis by using the GraphPad Prism software.

### 2.17. Molecular docking

Molecular docking was performed using AutoDock Vina (Eberhardt et al., 2021) and AutoDock-Tools (Morris et al., 2009) in order to theoretically study the interaction mode between oxaliplatin and NK. The crystal structure of NK (PDB:4DWW) was obtained from the RCSB Protein Data Bank (<https://www.pdb.org>), further removing water molecules, adding hydrogen bonds and calculating Gasteiger charges. The RESP atomic charge calculation, structure optimization and energy minimization of oxaliplatin were carried out by using ORCA (Neese, 2018) and Multiwfn (Helmich-Paris et al., 2021; Lu and Chen, 2012). The parameter files of protein and ligand structure were prepared by AutoDock Tools. Meanwhile, a Lamarckian genetic algorithm was selected for binding site search on NK, and other binding parameters to search entire NK. The visualization of docking result was realized by using Ligplot+ (Laskowski and Swindells, 2011) and PyMOL to analyze the binding site and binding energy of NK and oxaliplatin.

## 3. Results and discussion

### 3.1. Preparation of NK

The finished black soybean natto was shown in Fig. 1(a) and the elution curve for gel filtration chromatography in the purification and isolation of the NK was shown in Fig. S1.

### 3.2. Enzyme activity and preliminary structural investigation of NK

Thrombosis occurs is the result of a combination of multiple factors including coagulation, anticoagulation and the fibrinolytic system. Fibrin is the main component of a thrombus. In the blood, the fibrinolytic system is constantly activated in order to dissolve the newly produced fibrin and keep the blood in a state of equilibrium. It is worth mentioning that the thrombolytic ability of a drug is often measured by its effect on the fibrinolytic system and the level of fibrin degradation. So, we used the fibrin plate method to test the fibrinolytic activity of NK and the standard curve of the urokinase activity was shown in Table S1 and Fig. S2. In addition, the dissolving circle of NK on the fibrin plate was shown in Fig. 1(b), with a diameter of 3.4 cm. The results showed that NK had a strong fibrinolytic activity and the nattokinase activity of NK was calculated to be 600,391 U/g, which is medium in comparison with the reported reference (Ni et al., 2016; Liang et al., 2007).

The preliminary structure of NK was shown in Fig. 1(c) and Fig. 1(d), which investigated by infrared spectroscopy and scanning electron microscopy. The peak at  $1633.9 \text{ cm}^{-1}$  was a C = O bond stretching vibration peak (protein amide I) and the peak at  $1245.6 \text{ cm}^{-1}$  was a C-N bond stretching vibration peak (protein amide III), indicating that the

Table 2

IC<sub>50</sub> values of oxaliplatin alone and in combination with NK to cells for 48 h.

| Drug             | IC <sub>50</sub> (µM) |                |              |                |                           |
|------------------|-----------------------|----------------|--------------|----------------|---------------------------|
|                  | BGC-823               | HeLa           | HepG-2       | NCI-H460       | HUVEC                     |
| Oxaliplatin      | 11.29 ± 0.34          | 46.18 ± 3.25   | 12.45 ± 0.34 | 35.31 ± 0.43   | 12.37 ± 2.21              |
| Oxaliplatin + NK | 6.90 ± 2.29*          | 16.96 ± 0.21** | 7.40 ± 2.62* | 20.52 ± 0.68** | 9.61 ± 0.29 <sup>ns</sup> |
| FI               | 1.64                  | 2.72           | 1.68         | 1.72           | 1.29                      |

(FI: IC<sub>50</sub> of the group treated with oxaliplatin / IC<sub>50</sub> of the group treated with oxaliplatin and NK; \*P < 0.05; \*\*P < 0.01).

NK we isolated had the chemical structure of a protein. Under scanning electron microscopy, the NK had a rough surface and a clearly visible blocky structure with irregularly cleft edges. It remained the case under high magnification electron microscopy, where the surface appeared more compactly blocky and uneven, with mostly deep visible depressions. Fig. 1 (e) shows the SDS-PAGE results of NK, indicating a significant protein band at 28 kDa. Therefore, the molecular weight of NK can be preliminarily determined through SDS-PAGE, which is consistent with literature reports (Weng et al., 2017; Liang et al., 2007).

### 3.3. MTT assay

The MTT colorimetric method is a common test for determining cell viability, proliferation and cytotoxicity. As shown in Fig. 2, there was no significant difference in the survival rate of BGC-823, HeLa, HepG-2, NCI-H460, and HUVEC cells compared with the control group at the NK concentration of 125, 250, and 500 µg/mL. This result indicated that NK had no effect on the cell survival rate (>98 %). In other words, NK has been tested to have no significant cytotoxicity, which was consistent with predecessors' toxicology tests (Hogan et al., 2018), so we chose the median value of 250 µg/mL as the NK concentration for subsequent experiments.

In addition, studies have shown that Lentinan may be an ideal agent for the combination therapy of oxaliplatin against hepatocellular carcinoma (Zhang et al., 2016). There were also reports that genipin increased the oxaliplatin-induced cell death via p53-DRAM autophagy (Kim et al., 2020). Guo J et al have also demonstrated that GW4064 can synergistically enhance the anti-tumor effect of oxaliplatin in colon cancer cells (Guo et al., 2021a, 2021b). Given the previous experience of combining platinum drugs with other drugs, we also investigated the effects of oxaliplatin alone and in combination with NK on the apoptosis of BGC-823, HeLa, HepG-2, NCI-H460, and HUVEC cells. Cytotoxicity was expressed by IC<sub>50</sub> values. As seen in Table 2, oxaliplatin alone had a toxic effect on four kinds of cancer cells. In combination with NK, the IC<sub>50</sub> values decreased, which meant the cytotoxicity increased. When compared the fold increase (FI) values, the range of FI values is from 1.64 to 2.72, which showed the toxic effect of "OXA + NK" group on cancer cells increased significantly, but there was no significant increase in toxicity to HUVEC cells. The MTT results suggested that NK may have

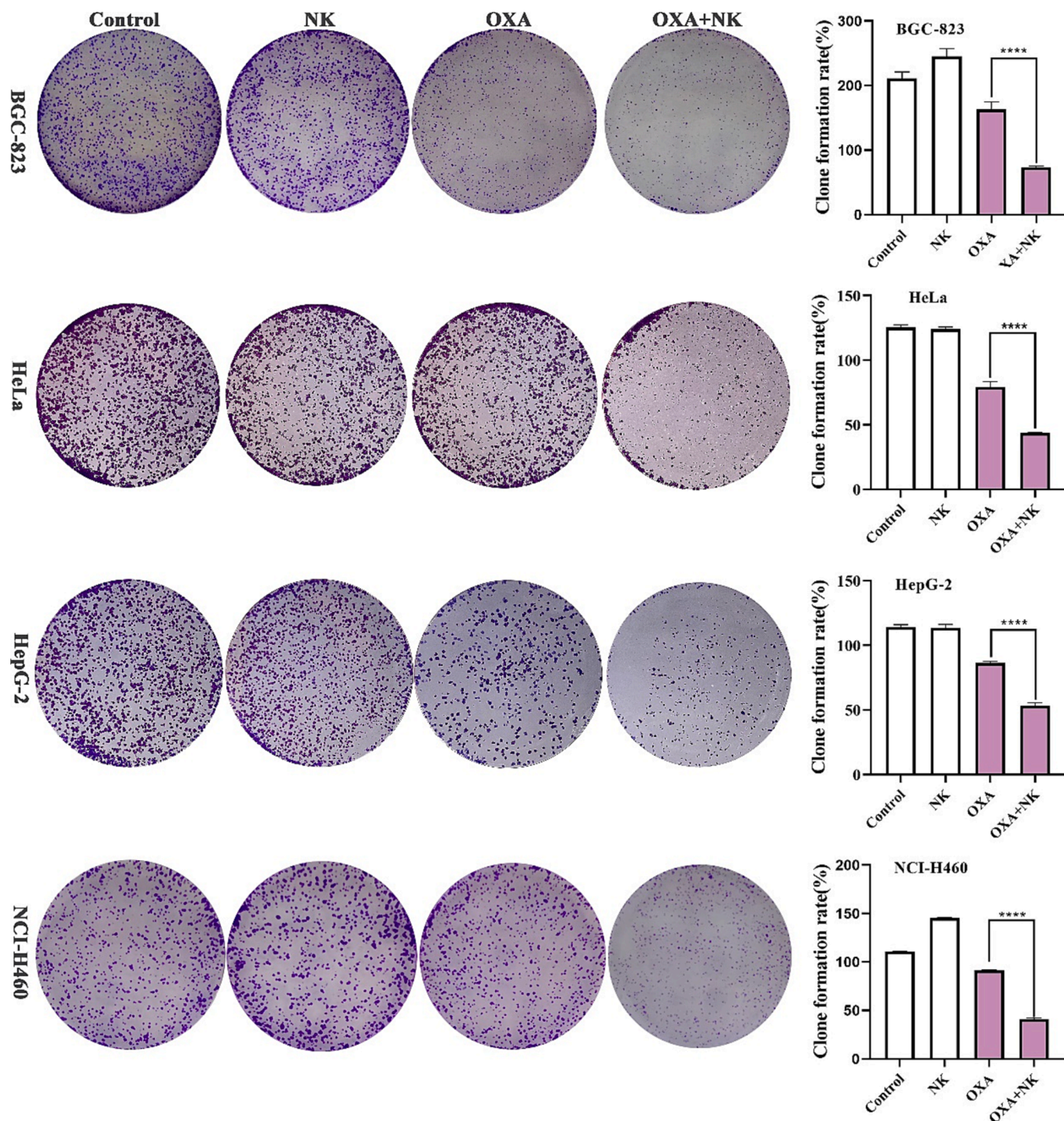


Fig. 3. Clone formation of oxaliplatin alone and in combination with NK to cells for 10 days, the concentrations of oxaliplatin to the four cells is corresponding  $IC_{50}$  values of oxaliplatin alone group, and the concentrations of NK is 250  $\mu\text{g}/\text{mL}$ . Histogram of clone formation rate is listed on the right (\*\*\*\* $P < 0.0001$ ).

synergistic anticancer effects with oxaliplatin without increasing the toxic effects on normal cells. We performed subsequent experiments with concentrations around the  $IC_{50}$  values.

### 3.4. Clone formation assay

The clone formation assay is an important classical method, used to analyze the effects on the proliferation of cells (Ren et al., 2022). As shown in Fig. 3, the number of cell clones in the oxaliplatin alone group was lower than that in the control and NK groups; and the number of cell clones in the combination group was significantly lower than that in the

oxaliplatin alone group. The number of clones in each group was counted and the clone formation rate was calculated, and the results showed that there was a significant difference (\*\*\*\* $P < 0.0001$ ) between the oxaliplatin alone group and the combination group. The above results indicated that the combination of oxaliplatin and NK inhibited the clone formation ability of cancer cells compared to oxaliplatin alone, which was consistent with the MTT results.

### 3.5. Hoechst 33342 staining

The Hoechst 33342 staining is a generic method for analyzing

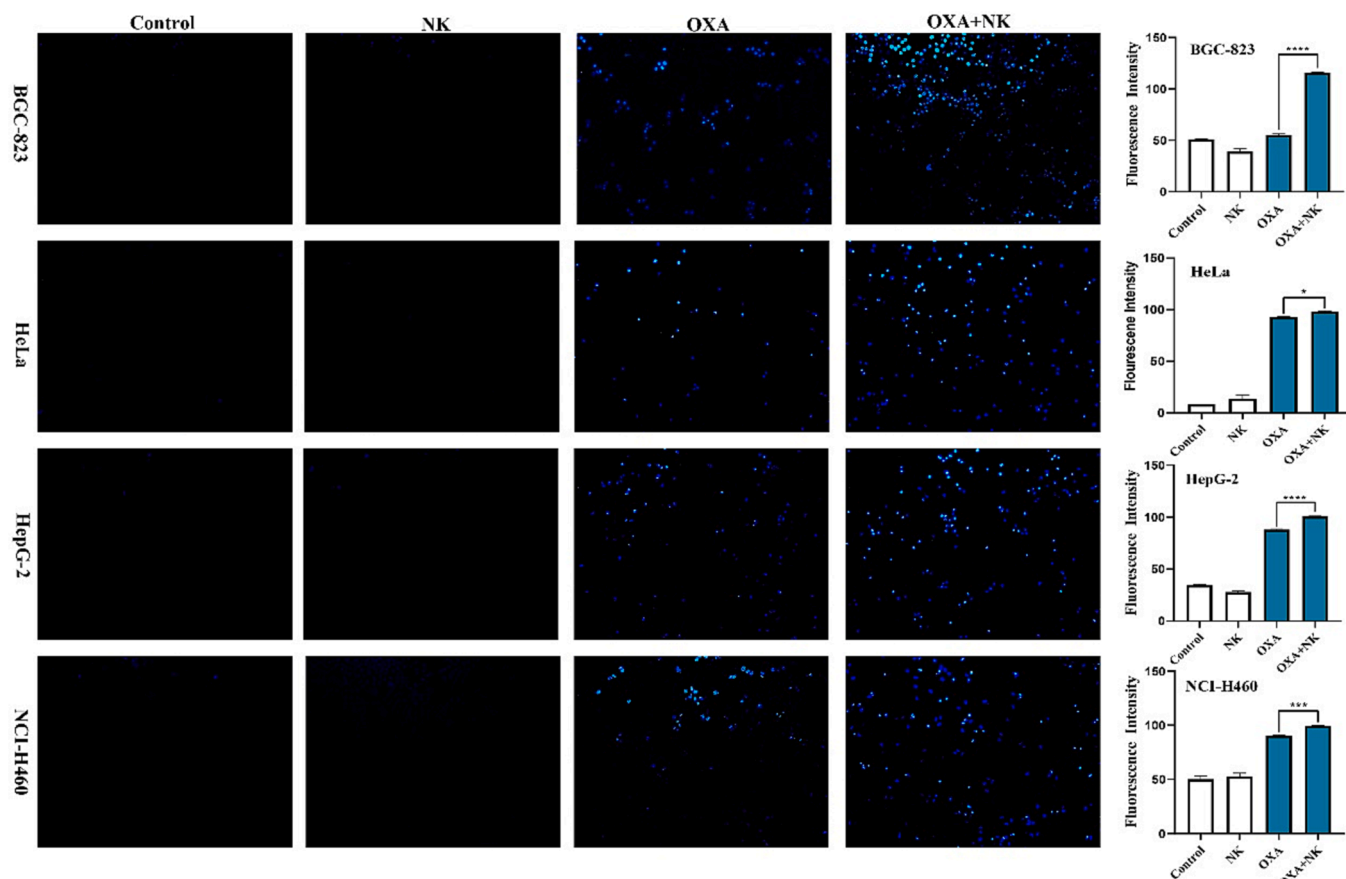


**Fig. 4.** Apoptotic morphology of oxaliplatin alone and in combination with NK to cells for 24 h ( $10 \times 10$ ), the concentrations of oxaliplatin to the four cells is corresponding  $IC_{50}$  values of oxaliplatin alone group, and the concentrations of NK is 250  $\mu\text{g}/\text{mL}$ . Histogram of average fluorescence intensity is listed on the right (\* $P < 0.05$ , \*\*\* $P < 0.001$ , \*\*\*\* $P < 0.0001$ ).

apoptotic effects on cancer cells. Cells that undergo apoptosis not only show morphology changes and cell shrinkage (Zhang et al., 2023a, 2023b) but also enhance the permeability of the cell membrane (Ji et al., 2019). In addition, increased permeability of the cell membrane leads to more dye entering the cell. The result of Hoechst 33,342 was shown in Fig. 4, the intensity of blue fluorescence was observed to determine whether apoptosis was occurring in the cells. After staining, there was almost no blue fluorescence in the control and NK groups. The cells in the oxaliplatin alone group started to shrink and appeared blue and bright blue fluorescence, and the shrinkage cells in the combination with NK group increased and appeared more blue and bright blue fluorescence. The relative fluorescence intensity of blue fluorescence was analyzed by Image J software, which showed significant differences (\* $P < 0.05$ , \*\*\* $P < 0.001$ , \*\*\*\* $P < 0.0001$ , respectively) between the oxaliplatin alone and combination with NK groups (Fig. 4). Therefore, after treatment with oxaliplatin alone, there was some apoptosis of cancer cells, but the proportion of apoptotic cells increased significantly after combination with NK, indicating that NK could enhance the anticancer effect of oxaliplatin.

### 3.6. DCFH-DA staining

Intracellular ROS levels are always assessed by DCFH-DA staining. ROS is one of the hallmarks of early apoptosis cells. Elevated levels of ROS cause non-fluorescent DCFH to change to green fluorescent DCF (Laggner et al., 2006). Fig. 5 showed the results of ROS levels, and we determined the intracellular ROS levels by observing and analyzing the intensity of green fluorescence. After staining, intracellular ROS levels in the control and NK groups were low and therefore the green

fluorescence was weak or even absent. After oxaliplatin stimulation alone, intracellular ROS levels increased and green fluorescence began to appear, and after combination with NK, green fluorescence was enhanced. The relative fluorescence intensity of green fluorescence was analyzed by Image J software, which showed that combination with NK increased intracellular ROS levels more significantly than oxaliplatin alone, indicated that there were significant differences (\* $P < 0.05$ , \*\* $P < 0.01$ , \*\*\*\* $P < 0.0001$ , respectively) between the two groups (Fig. 5). Based on the above results, we speculated that oxaliplatin may induce apoptosis by increasing intracellular ROS levels and that NK also achieved a synergistic anticancer effect.

### 3.7. JC-1 assay

The results of Hoechst 33342 and DCFH-DA staining suggested that oxaliplatin may have toxic effects on tumor cells by causing an elevation of intracellular ROS, resulting in mitochondrial dysfunction and ultimately apoptosis. To judge this conclusion, we measured the changes of mitochondrial membrane potential (MMP) using JC-1 as a fluorescent probe. JC-1, a cationic fluorescent dye, is well-known to characterize the MMP. In the presence of a high membrane potential, this dye exists in the mitochondria as aggregates with red fluorescence whereas at a low membrane potential it is a monomer with green fluorescence (Elefantova et al., 2018). The mitochondrial pathway represents one of the major pathways of cell apoptosis. If the MMP is depolarized, it will lead to mitochondrial damage, and ultimately lead to cell apoptosis (Cho and Sun, 2015).

As shown in Fig. 6, the control and NK groups had higher membrane potential, so they showed red fluorescence and almost no green

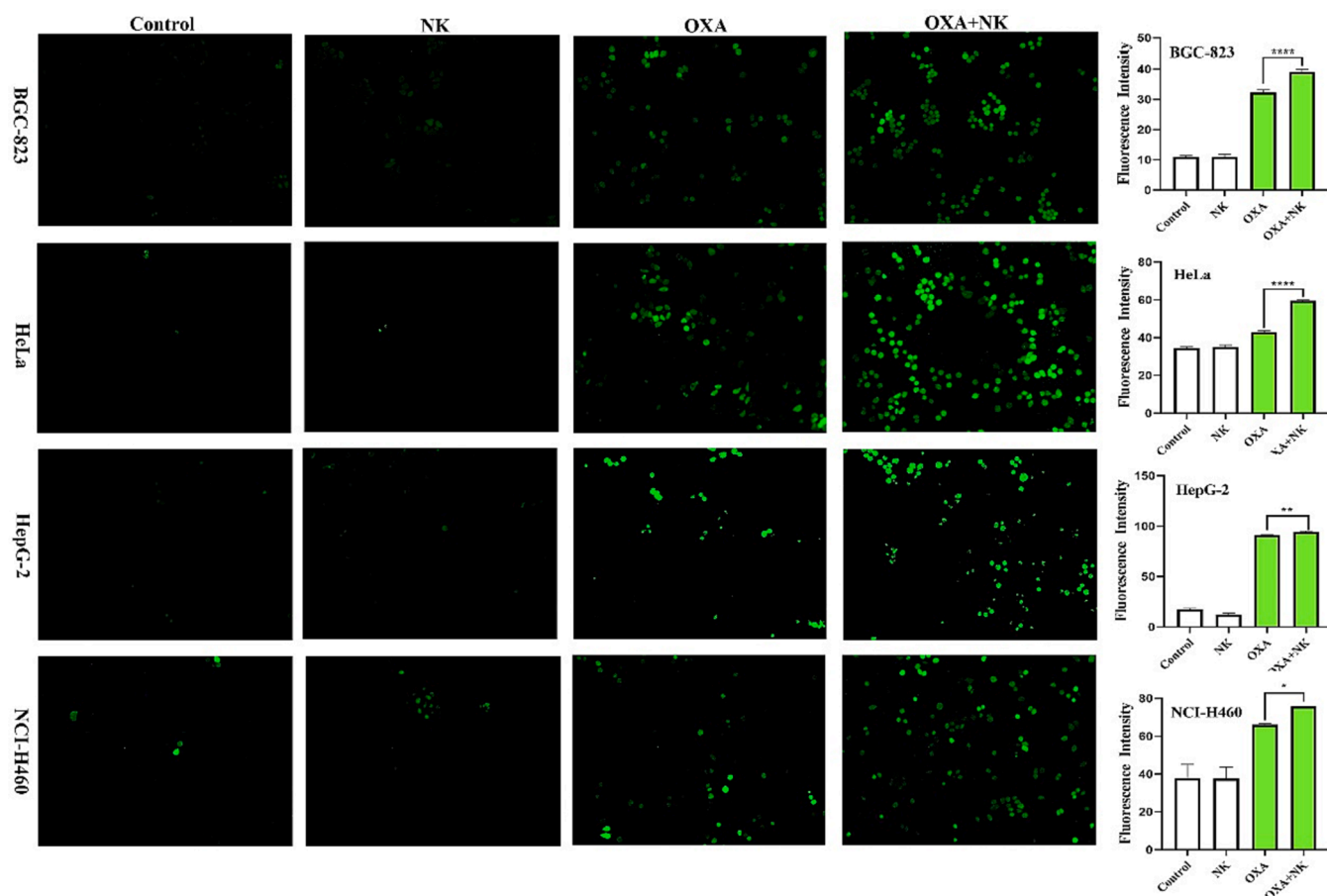


Fig. 5. ROS levels of oxaliplatin alone and in combination with NK to cells for 24 h ( $10 \times 10$ ), the concentrations of oxaliplatin to the four cells is corresponding  $IC_{50}$  values of oxaliplatin alone group, and the concentrations of NK is  $250 \mu\text{g}/\text{mL}$ . Histogram of average fluorescence intensity is listed on the right (\* $P < 0.05$ , \*\* $P < 0.01$ , \*\*\* $P < 0.0001$ ).

fluorescence. The addition of oxaliplatin resulted in a decrease in MMP, then the red fluorescence diminished and the green fluorescence increased. After combined with NK, there was almost no red fluorescence, but more green fluorescence. The relative fluorescence intensity of red or green fluorescence was analyzed by Image J software, which showed that the combination with NK group reduced the MMP more significantly compared to the oxaliplatin alone group, and indicated that there were significant differences (\* $P < 0.05$ , \*\* $P < 0.01$ , \*\*\* $P < 0.0001$ , respectively) between the two groups (Fig. 6). We therefore concluded that oxaliplatin may induce apoptosis via the mitochondrial pathway, with NK playing a synergistic role.

### 3.8. Cell cycle

During the process of cell growth, on the one hand, inducing apoptosis can inhibit cell proliferation, and on the other hand, blocking the cell cycle can also inhibit cell proliferation (Khan et al., 2022). Cell proliferation is inhibited most notably by disruption of the cell cycle. DNA plays a key role in the cell cycle as the main protagonist of the process. DNA damage directly leads to cell cycle arrest and thus interrupts cell growth and proliferation (Hegde et al., 2017). Therefore, in this paper, the effect of oxaliplatin on the cell cycle was investigated by FCM.

As shown in Fig. 7, the percentage of cells in S-phase appeared to be elevated in both groups of oxaliplatin alone and combination with NK compared to the control and NK groups, and the percentage of cells in S-phase was higher with the combination group than with oxaliplatin group. From this, it could be seen that oxaliplatin arrested the cell cycle

of BGC-823, HeLa, HepG-2, and NCI-H460 cells mainly in the S-phase, notably, the action of combination with NK on the S-phase was stronger than that of oxaliplatin alone. It suggested that its major effect on the cell cycle was to inhibit the phase of DNA synthesis (S-phase), which was consistent with those reported in the literature (Jing et al., 2018; Noordhuis et al., 2008).

### 3.9. Cellular uptake

After oxaliplatin enters the cell, platinum will form a Pt-DNA complex with DNA, making it impossible for the cell to replicate. The intracellular accumulation of platinum drugs is essential for producing the anticancer effect (Gao et al., 2019), and increasing the cellular uptake of oxaliplatin may be the key to improving the anticancer efficacy. Therefore, ICP-OES was chosen to detect the cellular uptake of oxaliplatin.

As shown in Table S2 and Fig. 8, the Pt content entering the cells was increased after the combination with NK, and the results were consistent with the cytotoxicity results. The results of this experiment showed that the combination of oxaliplatin and NK increased the accumulation of intracellular Pt content and thus inhibited cell viability, and further confirmed that oxaliplatin inhibited cell proliferation by affecting DNA synthesis.

### 3.10. Transwell migration and invasion assay

The migration and invasion of cancer cells are major factors of death in cancer patients. The transwell assay is the most frequent approach for

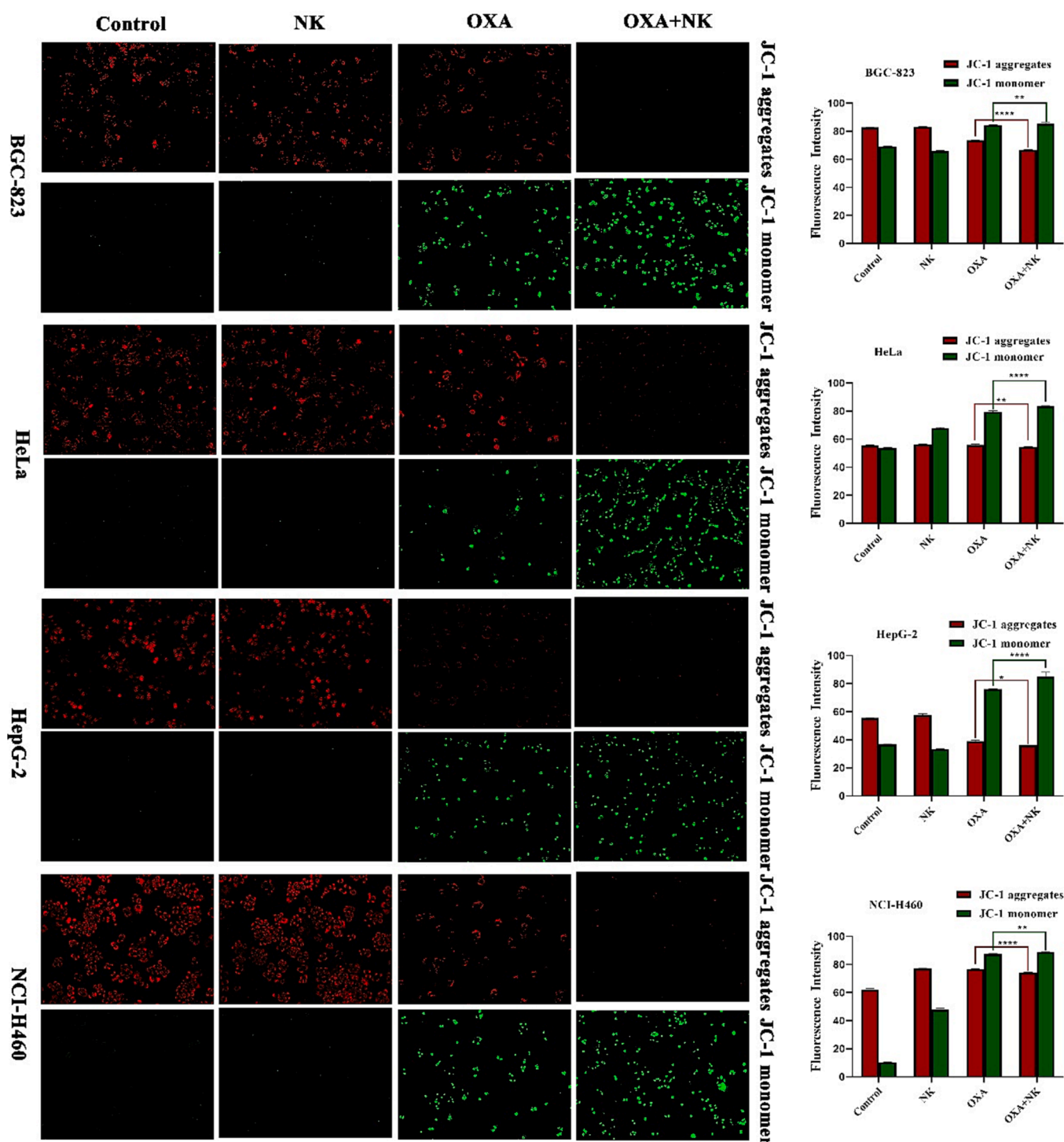


Fig. 6. MMP of oxaliplatin alone and in combination with NK to cells for 24 h ( $10 \times 10$ ), the concentrations of oxaliplatin to the four cells is corresponding  $IC_{50}$  values of oxaliplatin alone group, and the concentrations of NK is  $250 \mu\text{g/mL}$ . Histogram of average fluorescence intensity is listed on the right (\* $P < 0.05$ , \*\* $P < 0.01$ , \*\*\* $P < 0.0001$ ).

cell migration and invasion studies by detecting the number of cancer cells crossing the chamber membrane (Zhan et al., 2022).

The results of the cell migration and invasion assay were shown in Fig. 9. In the migration experiments, more cells in the control and NK groups reached the lower chamber due to induction by the high concentration of serum medium in the lower chamber. With the addition of oxaliplatin alone and in combination with NK, the number of cells reaching the lower chamber gradually decreased. This suggested that NK contributes to oxaliplatin inhibition of cancer cell migration. In the

invasion experiments, cancer cells needed to produce matrix metalloproteinases to digest the matrigel matrix in the upper chamber in order to reach the lower chamber from the upper chamber. The number of cells reaching the lower chamber in the control group and NK was still high, but the number has significantly decreased due to the effect of oxaliplatin alone and in combination with NK. Accordingly, it is suggested that oxaliplatin may inhibit the production of intracellular matrix metalloproteinases, making it impossible for cancer cells to cross the matrigel matrix and eventually inhibit their invasive ability. The

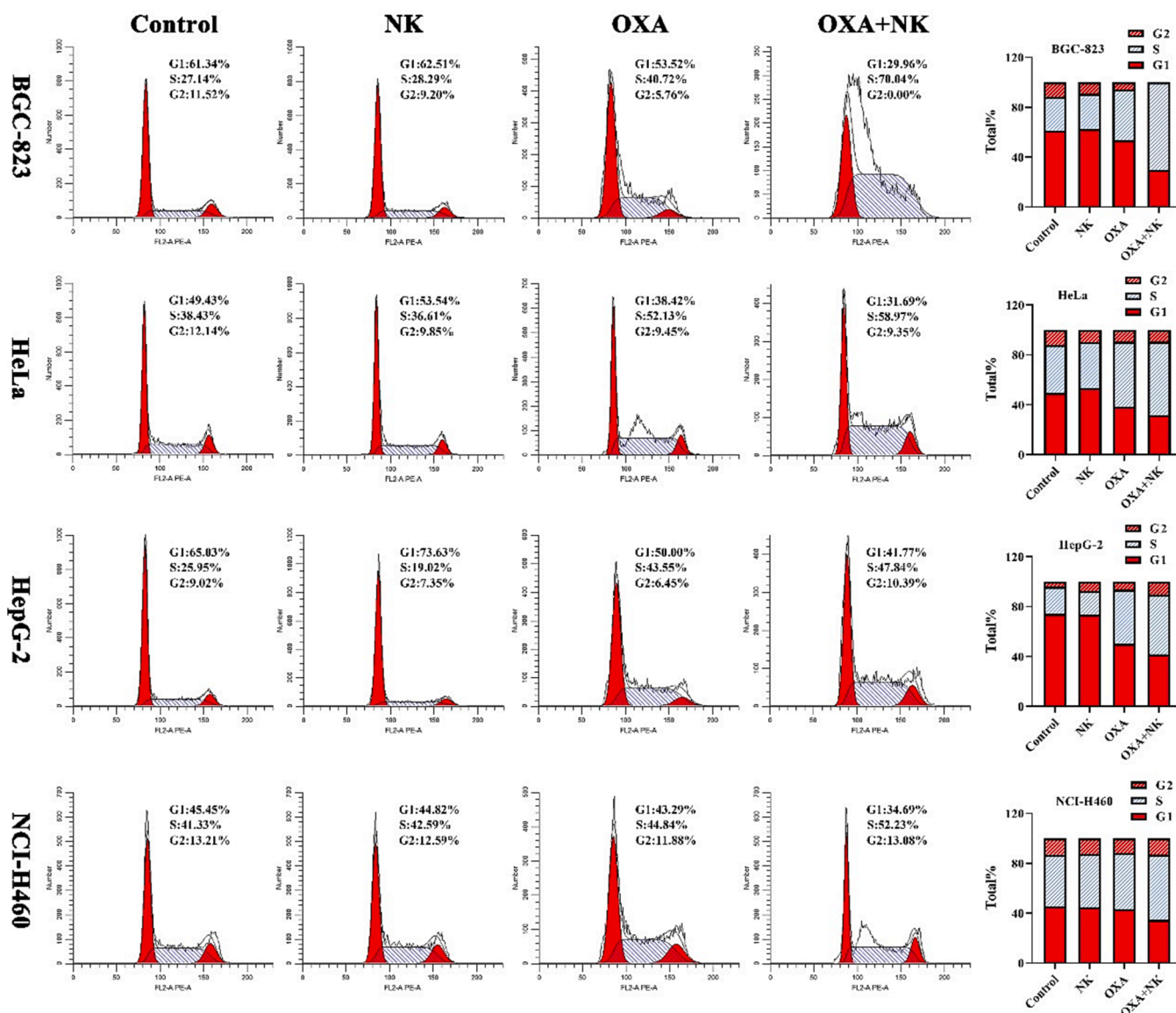


Fig. 7. Cell cycle of cells after incubation with oxaliplatin alone and in combination with NK for 24 h, the concentrations of oxaliplatin to the four cells is corresponding IC<sub>50</sub> values of oxaliplatin alone group, and the concentrations of NK is 250 µg/mL. Histogram of the cell cycle phase distribution is listed on the right.

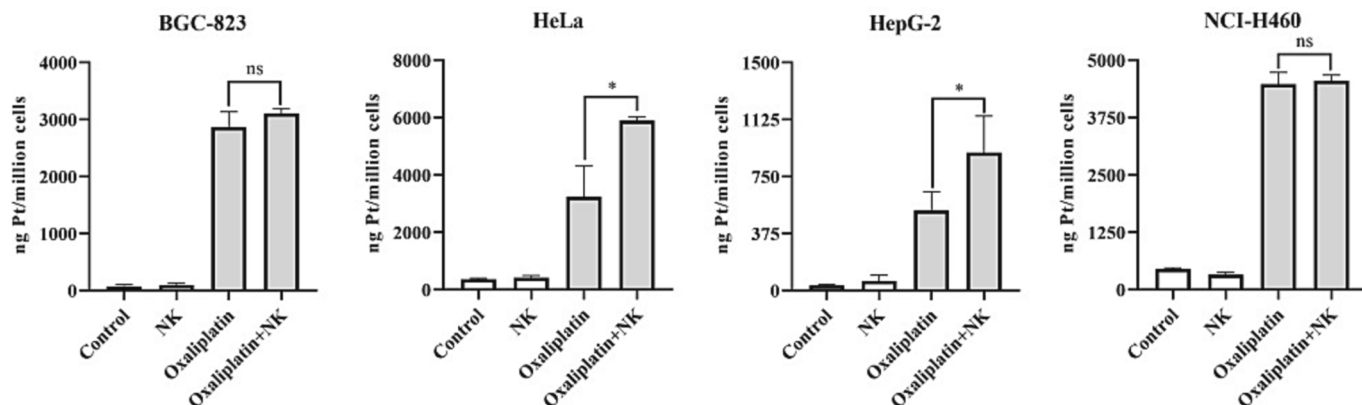
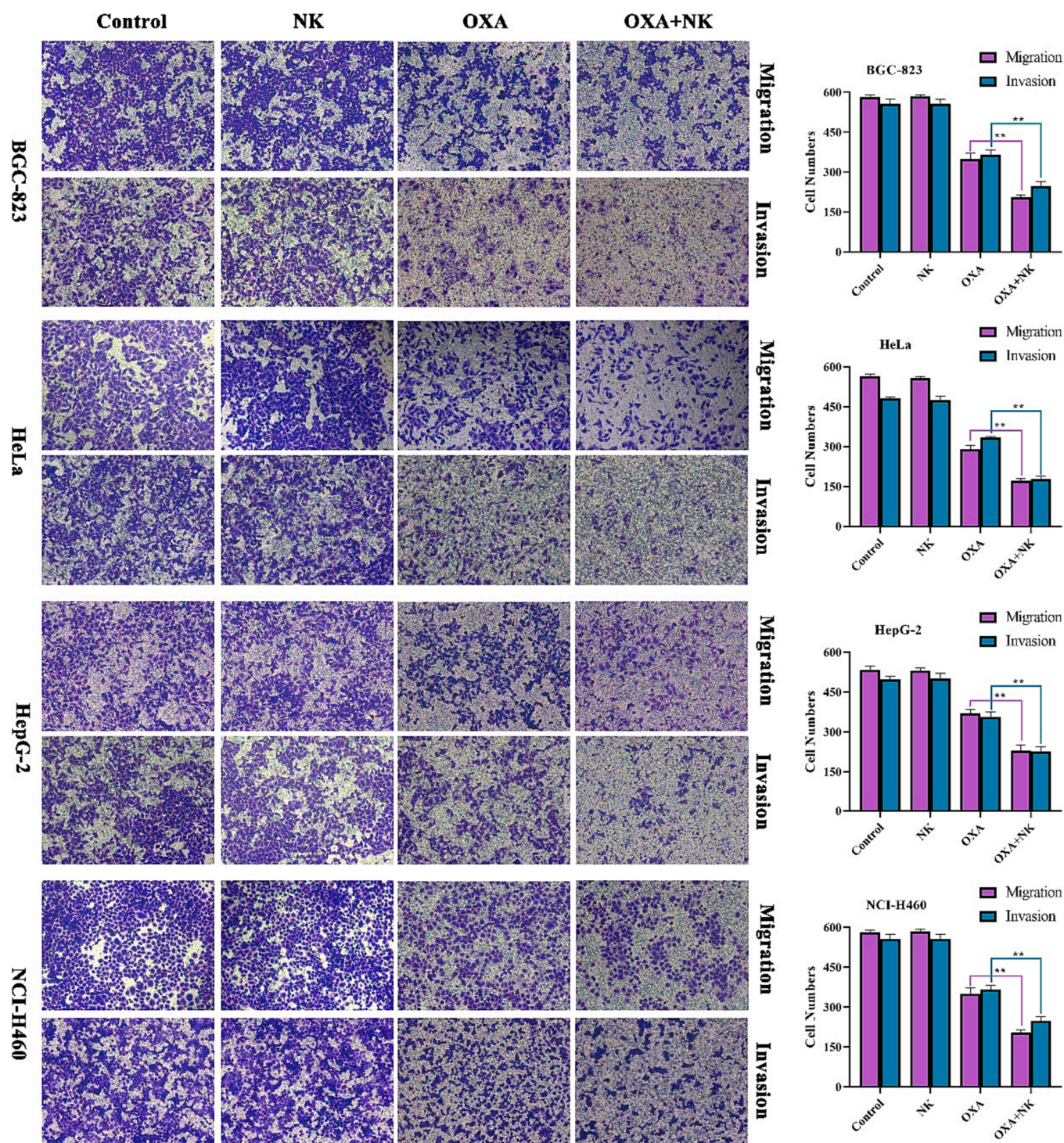


Fig. 8. Pt content of oxaliplatin alone and in combination with NK to cells for 24 h, the concentrations of oxaliplatin to the four cells is corresponding IC<sub>50</sub> values of oxaliplatin alone group, and the concentrations of NK is 250 µg/mL (\*P < 0.05; ns: no significance).



**Fig. 9.** Migration and invasion of oxaliplatin alone and in combination with NK to cells for 24 h ( $10 \times 10$ ), the concentrations of oxaliplatin to the four cells is corresponding  $IC_{50}$  values of oxaliplatin alone group, and the concentrations of NK is  $250 \mu\text{g/mL}$ . Histogram of cell numbers is listed on the right (\*\* $P < 0.01$ ).

number of cells reaching the lower chamber was counted by Image J software, which showed that the combination with NK group had a stronger effect on the migration and invasion ability of cancer cells, indicated that there were significant differences (\*\* $P < 0.01$ ) between the two groups of oxaliplatin alone and in combination with NK, and the addition of NK could significantly enhance the sensitivity of cancer cells to oxaliplatin. Therefore, we inferred that NK promoted oxaliplatin to inhibit the migration and invasion of cancer cells.

### 3.11. *In vitro* angiogenesis assay

An uncontrolled angiogenesis rate is routinely seen in cancer growth, resulting in rapid tumor growth. Inhibiting angiogenesis is one of the most significant anticancer strategies in terms of cancer cells migration and invasion (Astinfeshan et al., 2019).

As Fig. 10(a) showed that in the control and NK groups, the number of vascular lumens gradually increased and the structure became progressively more intact with increasing time. In the oxaliplatin alone

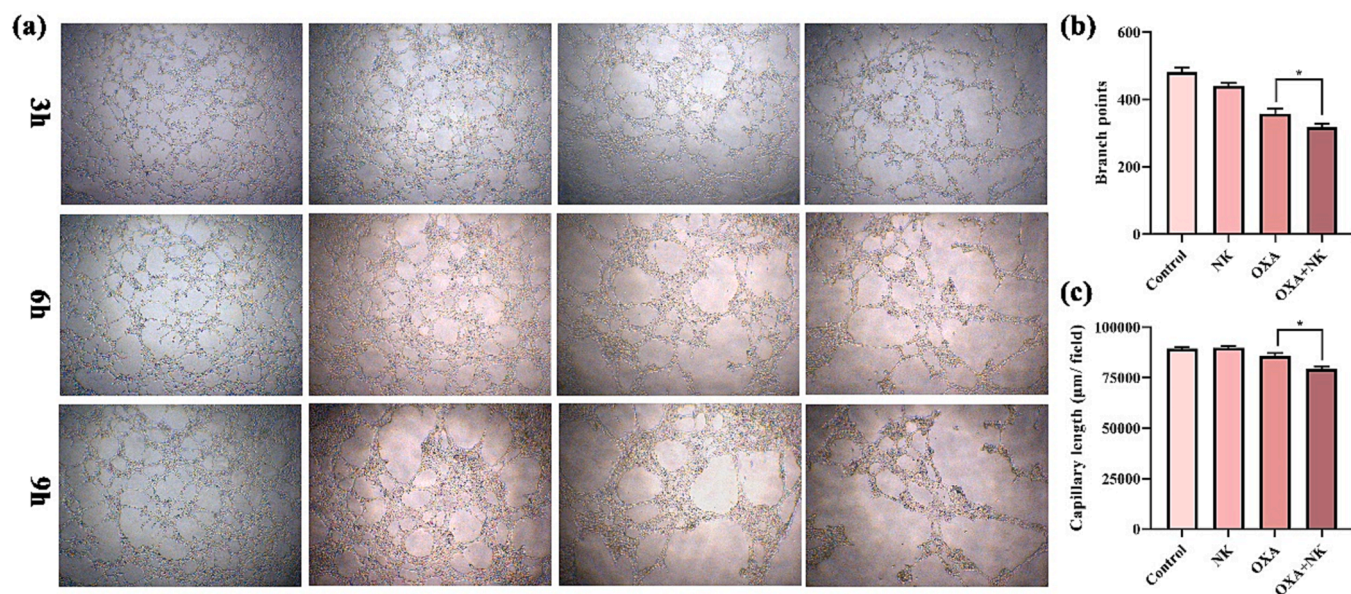


Fig. 10. (a) In vitro angiogenesis of oxaliplatin alone and in combination with NK to HUVEC cells at 3, 6, and 9 h, (b-c) Branch points and capillary length of oxaliplatin alone and in combination with NK to HUVEC cells at 9 h (\*P < 0.05), the concentrations of oxaliplatin is 10 µM, and the concentrations of NK is 250 µg/mL (10 × 4).

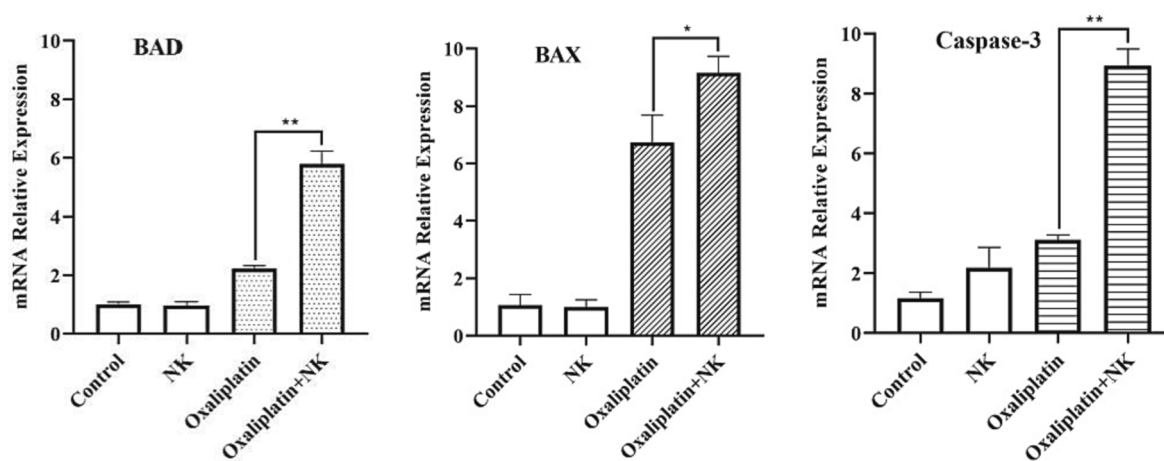


Fig. 11. Mrna expression of related genes after oxaliplatin alone and in combination with nk to bgc-823 cell for 24 h, the concentrations of oxaliplatin is 10 µM, and the concentrations of NK is 250 µg/mL (\*\*P < 0.01, \*P < 0.05).

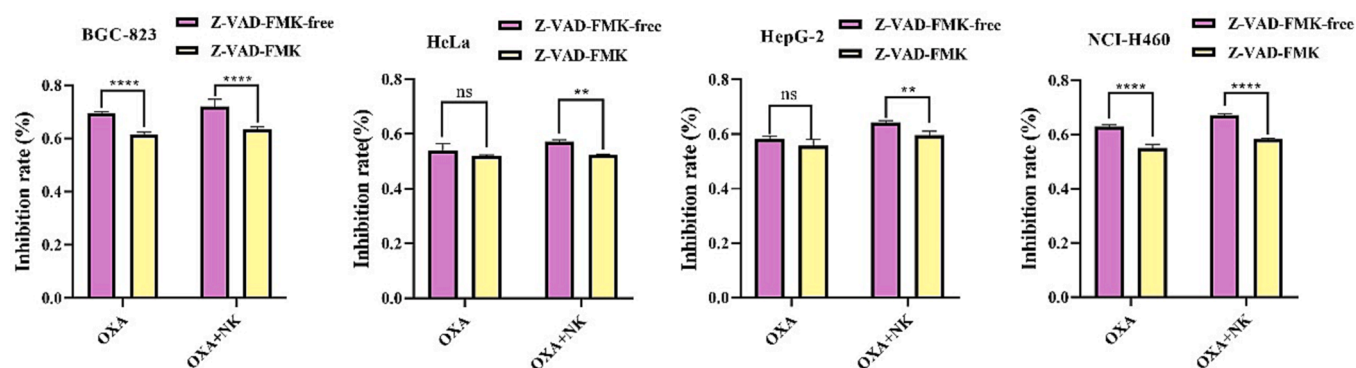
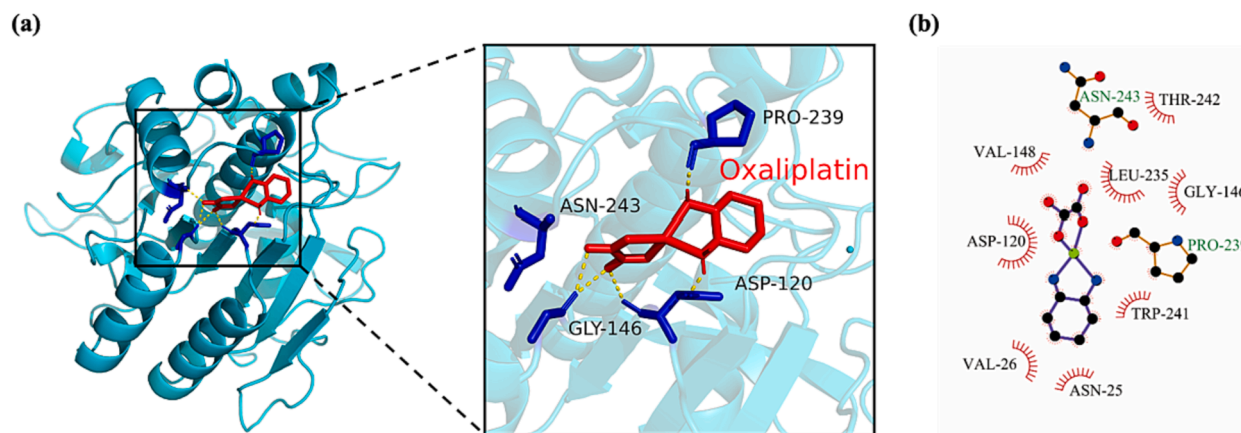


Fig. 12. The inhibition rate of different cells pretreated 10 h with 30 µM Z-VAD-FMK, then with and without nattokinase (250 µg/mL), Oxaliplatin concentration was selected to cell IC<sub>50</sub>, 30 µM OXA for HeLa cells and 20 µM OXA for the BGC-823, HepG-2, NCI-H460 cells, respectively (\*\*P < 0.01, \*\*\*\*P < 0.0001).



**Fig. 13.** (a) Docking analysis visualization of NK binding with Oxaliplatin. Amino acids that form hydrogen bonds are identified in blue while hydrogen bonds are shown in yellow. (b) The diagrammatic representation of the result of Ligplot analysis.

group, the number of vascular lumens decreased and the structure gradually shrunk. In the combination with NK group, the number of vascular lumens was minimal and the structure tent to dissolve. The number of branch points and the capillary length at 9 h were calculated and analyzed by using Image J software in Fig. 10 (b-c), which showed that after combination with NK, they were significantly lower than the oxaliplatin alone group, and indicated that there were significant differences ( $*p < 0.05$ ) between the two groups. We concluded that oxaliplatin may be able to inhibit the hematopoiesis of HUVEC cells tube formation and that NK enhanced its efficacy.

### 3.12. RT-qPCR

Cell apoptosis enters a continuous reaction process under the interaction of apoptotic regulatory molecules, ultimately inducing cell death, which involves the regulation of many intracellular genes and extracellular factors. Studies have shown that BAD (Bumbat et al., 2020), BAX (Saleh et al., 2022) and Caspase-3 (Yu et al., 2020) are all pro-apoptotic genes associated with apoptosis and have important roles in apoptosis. Therefore, we examined the expression levels of apoptosis-related genes BAD, BAX and Caspase-3 by RT-qPCR. The results were shown in Fig. 11. In BGC-823 cells, the expression of BAD, BAX and Caspase-3 genes in the oxaliplatin group and oxaliplatin + NK group were significantly higher compared with the control group and NK group, and there was a significant difference between the expression of genes in the oxaliplatin alone and in combination with NK group. The results of this experiment suggested that oxaliplatin combined with NK could inhibit the proliferation of cancer cells and thus induce apoptosis by regulating the expression levels of BAD, BAX and Caspase-3 genes, and the mechanism might be related to the upregulation of BAD, BAX and Caspase-3 genes.

### 3.13. Study on the apoptosis with Z-VAD-FMK

Z-VAD-FMK is an irreversible pan-caspase inhibitor could penetrate into the cells to inhibit apoptosis (Tsvetkov et al., 2022). As shown in Fig. 12, the inhibition rate of both NCI-H460 and BGC-832 cells alone and the combination group was significantly reduced after inhibitor action ( $****P < 0.0001$ ). However, for HeLa and HepG-2 cells, the inhibitor did not act significantly on oxaliplatin alone, but significantly reduced the inhibition rate of NK continuous group ( $**P < 0.01$ ), indicating that NK has a significant prominent effect on oxaliplatin to promote HeLa and HepG-2 cells. Obviously, either oxaliplatin alone or combined with NK induced cells inhibition was reduced by Z-VAD-FMK (30  $\mu$ M) treatment, this is consistent with the rise of caspase 3 expression as shown in the previous q-PCR experiment results.

### 3.14. Molecular docking

In order to study the interaction between oxaliplatin and NK, we detected the binding energy by AutoDockVina (Eberhardt et al., 2021), and selected the conformation with the lowest binding energy for molecular docking analysis. The docking result showed that Oxaliplatin was located in the outer surface groove near Asp 120, on the back of the NK substrate binding pocket, which implies that Oxaliplatin does not act as a competitive inhibitor of NK. The binding energy of NK to oxaliplatin is  $-6.4 \text{ kcal}\cdot\text{mol}^{-1}$ . As shown in Fig. 13(a), oxaliplatin can form hydrogen bonds with Asp 120, Gly 146, Asn 243 and Pro 239, respectively. In addition, LigPlot + analysis result shows that oxaliplatin not only forms hydrogen bonds with Asn 243 and Pro 239, but also contacts Asn 25, Val 26, Asp 120, Gly 146, Val 148, Trp 241 and Thr 242 through hydrophobic forces (Fig. 13b). These hydrophobic forces will further increase the stability of oxaliplatin and NK binding. In summary, NK has great potential as a carrier of oxaliplatin (Ghalandari et al., 2015). This is consistent with the previous results that the combination of NK and oxaliplatin enhanced the uptake of oxaliplatin by cancer cells.

## 4. Conclusion

In summary, NK isolated and purified from black soybean natto with nattokinase activity of 600,391 U/g, and has no significant cytotoxicity. Oxaliplatin could inhibit cell proliferation and oxaliplatin combined with NK could enhance its anticancer effect and lead to mitochondrial dysfunction by causing the increase of intracellular ROS, which eventually induced apoptosis. Oxaliplatin combined with NK also affected DNA synthesis by blocking cell cycles and improving cell uptake, ultimately inhibiting cell proliferation. In addition, they could also inhibit cell migration, invasion, and in vitro angiogenesis, thereby preventing the spread and metastasis of tumors. RT-qPCR showed that the mechanism of inhibition of cell proliferation and thus induction of apoptosis by the combination of NK and oxaliplatin may be achieved through the upregulation of BAD, BAX, and Caspase-3 genes. Molecular docking results show that NK could act as the carrier of oxaliplatin, which with binding energy of NK to oxaliplatin is  $-6.4 \text{ kcal}\cdot\text{mol}^{-1}$ . The above experimental results suggested that NK could enhance the sensitivity of cancer cells to oxaliplatin and play a synergistic role in the anticancer effect of oxaliplatin by inducing apoptosis through the mitochondrial pathway. It might provide a new therapeutic agent and pathway for cancer treatment, and may also provide a new field of application for NK.

## Declaration of competing interest

The authors declare that they have no known competing financial interests or personal relationships that could have appeared to influence the work reported in this paper.

## Acknowledgements

This work was supported by the Key R&D Projects of Shanxi (No. 201903D221036), the National Key Research and Development Program of China (No. 2021YFD1600601-2), breeding project of Shanxi Agricultural University (No. YZGC096) and the Central Guidance for Local Science and Technology Development Projects (No. YDZJSX2022A035).

## Appendix A. Supplementary data

Supplementary data to this article can be found online at <https://doi.org/10.1016/j.arabjc.2023.105478>.

## References

- Astinfeshan, M., Rasmi, Y., Kheradmand, F., Karimipour, M., Rahbarghazi, R., Aramwit, P., Nasirzadeh, M., Daeihassani, B., Shirpoor, A., Gholinejad, Z., 2019. Curcumin inhibits angiogenesis in endothelial cells using downregulation of the PI3K/Akt signaling pathway. *Food Biosci.* 29, 86–93.
- Astrup, T., Müllertz, S., 1952. The fibrin plate method for estimating fibrinolytic activity. *Arch. Biochem. Biophys.* 40, 346–351.
- Ayyagari, V.N., Hsieh, T.-H.J., Diaz-Sylvestre, P.L., Brard, L., 2017. Evaluation of the cytotoxicity of the Bithionol-cisplatin combination in a panel of human ovarian cancer cell lines. *BMC Cancer* 17, 49.
- Bumbat, M., Wang, M., Liang, W., Ye, P., Sun, W., Liu, B., 2020. Effects of Me2SO and trehalose on the cell viability, proliferation, and Bcl-2 family gene (BCL-2, BAX, and BAD) expression in cryopreserved human breast cancer cells. *Biopreserv. Biobank.* 18, 33–40.
- Chen, H., McGowan, E.M., Ren, N., Lal, S., Nassif, N., Shad-Kaneez, F., Qu, X., Lin, Y., 2018. Nattokinase: a promising alternative in prevention and treatment of cardiovascular diseases. *Biomarker Insights* 13, 1177271918785130.
- Cho, H.M., Sun, W., 2015. Control of mitochondrial dynamics by fas-induced caspase-8 activation in hippocampal neurons. *Exp. Neurobiol.* 24, 219–225.
- Devi, C.S., Mohanasrinivasan, V., Sharma, P., Das, D., Vaishnavi, B., Naine, S.J., 2016. Production, purification and stability studies on nattokinase: A therapeutic protein extracted from mutant *Pseudomonas aeruginosa* CMSS isolated from bovine milk. *Int. J. Pept. Res. Ther.* 22, 263–269.
- Eberhardt, J., Santos-Martins, D., Tillack, A.F., Forli, S., 2021. AutoDock Vina 1.2.0: New Docking Methods, Expanded Force Field, and Python Bindings. *J. Chem. Inf. Model.* 61, 3891–3898.
- Elefantova, K., Lakatos, B., Kubickova, J., Sulova, Z., Breier, A., 2018. Detection of the mitochondrial membrane potential by the cationic dye JC-1 in L1210 cells with massive overexpression of the plasma membrane ABCB1 drug transporter. *Int. J. Mol. Sci.* 19, 1985.
- Freites-Martinez, A., Shapiro, J., van den Hurk, C., Goldfarb, S., Jimenez, J.J., Rossi, A.M., Paus, R., Lacouture, M.E., 2019. Hair disorders in cancer survivors. *J. Am. Acad. Dermatol.* 80, 1199–1213.
- Gao, F., Xu, J.-C., You, X.-R., Gao, X., Wei, J.-L., Li, S.-X., Zhu, C.-L., Yang, C., 2019. The biological functions of LGR5 in promoting non-small cell lung cancer progression. *Transl. Cancer Res.* 8, 203–211.
- Ghalandari, B., Divsalar, A., Eslami-Moghadam, M., Saboury, A.A., Haertlé, T., Amanlou, M., Parivar, K., 2015. Probing of the interaction between  $\beta$ -lactoglobulin and the anticancer drug oxaliplatin. *Appl. Biochem. Biotechnol.* 175, 974–987.
- Grover, S.P., Hisada, Y.M., Kasthuri, R.S., Reeves, B.N., Mackman, N., 2021. Cancer therapy-associated thrombosis. *Arterioscler. Throm. Vas.* 41, 1291–1305.
- Guo, C.-X., Huang, X., Xu, J., Zhang, X.-Z., Shen, Y.-N., Liang, T.-B., Bai, X.-L., 2021a. Combined targeted therapy and immunotherapy for cancer treatment. *World J. Clin. Cases* 9, 7643.
- Guo, J., Zheng, J., Mu, M., Chen, Z., Xu, Z., Zhao, C., Yang, K., Qin, X., Sun, X., Yu, J., 2021b. GW4064 enhances the chemosensitivity of colorectal cancer to oxaliplatin by inducing pyroptosis. *Biochem. Biophys. Res. Commun.* 548, 60–66.
- He, P., Liu, X., Lou, Y., Gong, S., Cao, L., 2022. miR-34a-5p enhances the sensitivity of cervical cancer cells to oxaliplatin chemotherapy via targeting MDM4. *Clin. Exp. Obstet. Gyn.* 49, 54.
- Hegde, M., Vartak, S.V., Kavitha, C.V., Ananda, H., Prasanna, D.S., Gopalakrishnan, V., Choudhary, B., Rangappa, K.S., Raghavan, S.C., 2017. A benzothiazole derivative (5g) induces DNA damage and potent G2/M arrest in cancer cells. *Sci. Rep.* 7, 2533.
- Helmich-Paris, B., de Souza, B., Neese, F., Izsak, R., 2021. An improved chain of spheres for exchange algorithm. *J. Chem. Phys.* 155, 104109.
- Hodis, H.N., Mack, W.J., Meiselman, H.J., Kalra, V., Liebman, H., Hwang-Levine, J., Dustin, L., Kono, N., Mert, M., Wenby, R.B., 2021. Nattokinase atherothrombotic prevention study: a randomized controlled trial. *Clin. Hemorheol. Micro.* 78, 339–353.
- Hogan, S., O'Gara, J.P., O'Neill, E., 2018. Novel treatment of *Staphylococcus aureus* device-related infections using fibrinolytic agents. *Antimicrob. Agents Chemother.* 62, e02008-17.
- Ji, H.-Y., Yu, J., Liu, A.-J., 2019. Seleno- $\beta$ -lactoglobulin (Se- $\beta$ -Lg) induces mitochondria-dependent apoptosis in HepG2 cells. *Mol. Bio. Rep.* 46, 5025–5031.
- Jin, Y., Huang, Y., Chen, P., 2020. ANXA3 deletion inhibits the resistance of lung cancer cells to oxaliplatin. *Eur. Rev. Med. Pharmacol. Sci.* 24, 3741–3748.
- Jing, W., Song, N., Liu, Y., Qu, X., Hou, K., Yang, X., Che, X., 2018. DNA methyltransferase 3a modulates chemosensitivity to gemcitabine and oxaliplatin via CHK1 and AKT in p53-deficient pancreatic cancer cells. *Mol. Med. Rep.* 17, 117–124.
- Khan, H., Alam, W., Alsharif, K.F., Aschner, M., Pervez, S., Saso, L., 2022. Alkaloids and colon cancer: molecular mechanisms and therapeutic implications for cell cycle arrest. *Molecules* 27, 920.
- Kim, B.R., Jeong, Y.A., Kim, D.Y., Kim, J.L., Jeong, S., Na, Y.J., Yun, H.K., Park, S.H., Jo, M.L., Ashktorab, H., Smoot, D.T., Lee, D.-H., Oh, S.C., 2020. Genipin increases oxaliplatin-induced cell death through autophagy in gastric cancer. *J. Cancer* 11, 460–467.
- Kiss, N., Symons, K., Hewitt, J., Davis, H., Ting, C., Lee, A., Boltong, A., Tucker, R.M., Tan, S.-Y., 2021. Taste function in adults undergoing cancer radiotherapy or chemotherapy, and implications for nutrition management: a systematic review. *J. Acad. Nutr. Diet.* 21, 278–304.
- Laggner, H., Hermann, M., Gmeiner, B.M., Kapiotis, S., 2006. Cu<sup>2+</sup> and Cu<sup>+</sup> bathocuproine disulfonate complexes promote the oxidation of the ROS-detecting compound dichlorofluorescein (DCFH). *Anal. Bioanal. Chem.* 385, 959–961.
- Laskowski, R.A., Swindells, M.B., 2011. LigPlot+: multiple ligand-protein interaction diagrams for drug discovery. *J. Chem. Inf. Model.* 51, 2778–2786.
- Leal, A.C., Mizurini, D.M., Gomes, T., Rocha, N.C., Saraiva, E.M., Dias, M.S., Werneck, C.C., Sielski, M.S., Vicente, C.P., Monteiro, R.Q., 2017. Tumor-derived exosomes induce the formation of neutrophil extracellular traps: implications for the establishment of cancer-associated thrombosis. *Sci. Rep.* 7, 6438.
- Liang, X., Jia, S., Sun, Y., Chen, M., Chen, X., Zhong, J., Huan, L., 2007. secretory expression of nattokinase from *Bacillus subtilis* YF38 in *Escherichia coli*. *Mol. Biotechnol.* 37, 187–194.
- Liu, S., Gong, Y., Xu, X.D., Shen, H., Gao, S., Bao, H.D., Guo, S.B., Yu, X.F., Gong, J., 2021. MicroRNA-936/ERBB4/Akt axis exhibits anticancer properties of gastric cancer through inhibition of cell proliferation, migration, and invasion. *Kaohsiung J. Med. Sci.* 37, 111–120.
- Liu, R., Xu, B., Ma, Z., Ye, H., Guan, X., Ke, Y., Xiang, Z., Shi, Q., 2022. Controlled release of nitric oxide for enhanced tumor drug delivery and reduction of thrombosis risk. *RSC Adv.* 12, 32355–32364.
- Lu, T., Chen, F.W., 2012. Multiwfn: a multifunctional wavefunction analyzer. *J. Comput. Chem.* 33, 580–592.
- Luo, L., Ran, R., Yao, J., Zhang, F., Xing, M., Jin, M., Wang, L., Zhang, T., 2019. Se-enriched cordyceps militaris inhibits cell proliferation, induces cell apoptosis, and causes G2/M phase arrest in human non-small cell lung cancer cells. *Oncotargets Ther.* 12, 8751–8763.
- Modi, S., Arora, N., Dudeja, V., Banerjee, S., Saluja, A., 2015. 224 Efficacy of minnelide and oxaliplatin combination against pancreatic cancer. *Gastroenterology (New York, NY 1943)* 148, 1104–1105.
- Morris, G.M., Huey, R., Lindstrom, W., Sanner, M.F., Bewle, R.K., Goodsell, D.S., Olson, A.J., 2009. AutoDock4 and AutoDockTools4: automated docking with selective receptor flexibility. *J. Comput. Chem.* 30, 2785–2791.
- Mowaka, S., Linscheid, M., 2008. Separation and characterization of oxaliplatin dinucleotides from DNA using HPLC-ESI ion trap mass spectrometry. *Anal. Bioanal. Chem.* 392, 819–830.
- Neese, F., 2018. Software update: the ORCA program system, version 4.0. *WIREs Comput. Mol. Sci.* 8, e1327.
- Ni, H., Guo, P.-C., Jiang, W.-L., Fan, X.-M., Luo, X.-Y., Li, H.-H., 2016. Expression of nattokinase in *Escherichia coli* and renaturation of its inclusion body. *J. Biotechnol.* 231, 65–71.
- Noordhuis, P., Laan, A.C., van de Born, K., Losekoot, N., Kathmann, I., Peters, G.J., 2008. Oxaliplatin activity in selected and unselected human ovarian and colorectal cancer cell lines. *Biochem. Pharmacol.* 76, 53–61.
- Pearson, R.A., Wicha, S.G., Okour, M., 2023. Drug combination modeling: methods and applications in drug development. *J. Clin. Pharmacol.* 63, 151–165.
- Petrella, F., Rizzo, S., Casiraghi, M., Bardoni, C., Mohamed, S., Musso, V., Simonini, E., Spaggiari, L., 2022. State of the art and new perspectives in surgical treatment of lung cancer: a narrative review. *Transl. Cancer Res.* 11, 3869–3875.
- Prodger, A., Saha, P., Smith, A., Evans, C.E., 2016. Cancer-associated thrombosis: regulatory mechanisms and emerging directions. *Thrombosis Embolism: Res. Clin. Pract.* 906, 115–122.
- Ren, J., Hu, P., Ma, E., Zhou, X., Wang, W., Zheng, S., Wang, H., 2022. Enzyme-powered nanomotors with enhanced cell uptake and lysosomal escape for combined therapy of cancer. *Appl. Mater. Today* 27, 101445.
- Rickles, F.R., 2006. Mechanisms of cancer-induced thrombosis in cancer. *Pathophysiol. Haemo. t.* 35, 103–110.
- Ruhlmann, C.H., Herrstedt, J., 2016. New treatments on the horizon for chemoradiotherapy-induced nausea and vomiting. *Expert Opin. Pharmacol.* 17, 1623–1629.
- Safwat, G.M., Hassanin, K., Mohammed, E.T., Ahmed, E.K., Abdel Rhein, M.R., Ameen, M.A., Abdel-Aziz, M., Gouda, A.M., Peluso, I., Almeer, R., 2021. Synthesis, anticancer assessment, and molecular docking of novel chalcone-thienopyrimidine derivatives in HepG2 and MCF-7 cell lines. *Oxid. Med. Cell. Longev.* 2021, 4759821.

- Sahyon, H.A.E., Ramadan, E.N., Althobaiti, F., Mashaly, M., 2022. Anti-proliferative effects of the combination of Sulfamethoxazole and Quercetin via caspase3 and NFkB gene regulation: an in vitro and in vivo study. *Naunyn Schmiedebergs Arch. Pharmacol.* 395, 227–246.
- Saleh, K.K., Kirbag, S., Dalkılıç, S., 2022. Inhibitory effects of terfezia (Ascomycota) desert truffles on PANC-1 cell growth via upregulation of proapoptotic genes TP53, CDKN1A, and BAX and downregulation of antiapoptotic gene BCL2. *Int. J. Med. Mushrooms* 24, 61–70.
- Sato, A., 2015. Introduction of oxaliplatin for treating unresectable advanced or recurrent gastric cancer in clinical practice. *Gan to Kagaku ryoho. Cancer Chemother.* 42, 443–446.
- Sheng, Y., Yang, J., Wang, C., Sun, X., Yan, L., 2023. Microbial nattokinase: from synthesis to potential application. *Food Func.* 14, 2568–2585.
- Sung, H., Ferlay, J., Siegel, R.L., Laversanne, M., Soerjomataram, I., Jemal, A., Bray, F., 2021. Global cancer statistics 2020: GLOBOCAN estimates of incidence and mortality worldwide for 36 cancers in 185 countries. *CA: Cancer J. Clin.* 71, 209–249.
- Thun, M.J., DeLancey, J.O., Center, M.M., Jemal, A., Ward, E.M., 2010. The global burden of cancer: priorities for prevention. *Carcinogenesis* 31, 100–110.
- Tsvetkov, P., Coy, S., Petrova, B., Dreishpoon, M., Verma, A., Abdusamad, M., Rossen, J., Joesch-Cohen, L., Humeidi, R., Spangler, R.D., Eaton, J.K., Frenkel, E., Kocak, M., Corsello, S.M., Lutsenko, S., Kanarek, N., Santagata, S., Golub, T.R., 2022. Copper induces cell death by targeting lipoylated TCA cycle proteins. *Science* 375, 1254–1261.
- Wang, Z., Zhou, J., Fan, J., Qiu, S.-J., Yu, Y., Huang, X.-W., Sun, J., Tan, C.-J., Dai, Z., 2009. Oxaliplatin induces apoptosis in hepatocellular carcinoma cells and inhibits tumor growth. *Expert Opin. Inv. Drug.* 18, 1595–1604.
- Weng, Y., Yao, J., Sparks, S., Wang, K.Y., 2017. Nattokinase: an oral antithrombotic agent for the prevention of cardiovascular disease. *Int. J. Mol. Sci.* 18, 523.
- Xu, Y., Jiang, N., Yu, H., 2010. Effect of glutathione combined with cisplatin and oxaliplatin on the proliferation and apoptosis of lung carcinoma cell line. *Toxicol. Mech. Method.* 20, 487–492.
- Yan, G., Shu, M., Shen, W., Ma, L., Zhai, C., Wang, Y., Huang, Z., 2021. Heterologous expression of nattokinase from *B. subtilis natto* using *Pichia pastoris* GS115 and assessment of its thrombolytic activity. *BMC Biotechnol.* 21, 49.
- Yang, J., Wang, R., Feng, Q., Wang, Y.-X., Zhang, Y.-Y., Wu, W.-H., Ge, P.-L., Qi, J.-P., 2018. Safflower polysaccharide induces cervical cancer cell apoptosis via inhibition of the PI3K/Akt pathway. *S. Afr. J. Bot.* 118, 209–215.
- Yu, T., An, Q., Cao, X.-L., Yang, H., Cui, J., Li, Z.-J., Xiao, G., 2020. GOLPH3 inhibition reverses oxaliplatin resistance of colon cancer cells via suppression of PI3K/AKT/mTOR pathway. *Life Sci.* 260, 118294.
- Zhan, Q.-Q., Liu, Q.-Y., Yang, X., Ge, Y.-H., Xu, L., Ding, G.-Y., Guo, S., Zhu, B., Xu, W.-G., 2022. Effects of silencing neuropilin-2 on proliferation, migration, and invasion of colorectal cancer HT-29. *Bioengineered* 13, 11042–11049.
- Zhang, Y.-P., He, Q., Zhou, X.-H., Liu, G.-H., Yue, A.-Q., Gao, C.-Y., Zhao, J.-Z., Du, W.-J., Yan, S.-P., 2023b. In situ reduction synthesis of quinoline-based copper(I) complexes: “Self-activating” chemical nuclease, antioxidation and anticancer activity. *J. Mol. Struct.* 1292, 136090.
- Zhang, Y., Li, Q., Wang, J., Cheng, F., Huang, X., Cheng, Y., Wang, K., 2016. Polysaccharide from *Lentinus edodes* combined with oxaliplatin possesses the synergy and attenuation effect in hepatocellular carcinoma. *Cancer Lett.* 377, 117–125.
- Zhang, Y., Li, Y., Han, Z., Wang, D., Fu, Q., Umar Shinge, S.A., Mulu, T.A., Lu, X., 2022. Combined Immunotherapy and Targeted Therapies for Cancer Treatment: recent advances and future perspectives. *Curr. Cancer Drug Tar.* 23, 251–264.
- Zhang, Y., Pei, P., Zhou, H., Xie, Y., Yang, S., Shen, W., Hu, L., Zhang, Y., Liu, T., Yang, K., 2023a. Nattokinase-mediated regulation of tumor physical microenvironment to enhance chemotherapy, radiotherapy, and CAR-T therapy of solid tumor. *ACS Nano* 17, 7475–7486.